


RESEARCH

Open Access



# Assessment of endothelial colony forming cells delivery routes in a murine model of critical limb threatening ischemia using an optimized cell tracking approach

Marta Rojas-Torres<sup>1,2†</sup>, Ismael Sánchez-Gomar<sup>1,2†</sup>, Antonio Rosal-Vela<sup>1,2</sup>, Lucía Beltrán-Camacho<sup>1,2</sup>, Sara Eslava-Alcón<sup>1,2</sup>, José Ángel Alonso-Piñeiro<sup>1,2</sup>, Javier Martín-Ramírez<sup>3</sup>, Rafael Moreno-Luna<sup>4</sup> and Ma Carmen Durán-Ruiz<sup>1,2\*</sup> 

## Abstract

**Background:** Endothelial colony forming cells (ECFCs), alone or in combination with mesenchymal stem cells, have been selected as potential therapeutic candidates for critical limb-threatening ischemia (CLTI), mainly for those patients considered as “no-option,” due to their capability to enhance revascularization and perfusion recovery of ischemic tissues. Nevertheless, prior to translating cell therapy to the clinic, biodistribution assays are required by regulatory guidelines to ensure biosafety as well as to discard undesired systemic translocations. Different approaches, from imaging technologies to qPCR-based methods, are currently applied.

**Methods:** In the current study, we have optimized a cell-tracking assay based on DiR fluorescent cell labeling and near-infrared detection for in vivo and ex vivo assays. Briefly, an improved protocol for DiR staining was set up, by incubation of ECFCs with 6.67  $\mu$ M DiR and intensive washing steps prior cell administration. The minimal signal detected for the residual DiR, remaining after these washes, was considered as a baseline signal to estimate cell amounts correlated to the DiR intensity values registered in vivo. Besides, several assays were also performed to determine any potential effect of DiR over ECFCs functionality. Furthermore, the optimized protocol was applied in combination with qPCR amplification of specific human Alu sequences to assess the final distribution of ECFCs after intramuscular or intravenous administration to a murine model of CLTI.

**Results:** The optimized DiR labeling protocol indicated that ECFCs administered intramuscularly remained mainly within the hind limb muscle while cells injected intravenously were found in the spleen, liver and lungs.

**Conclusion:** Overall, the combination of DiR labeling and qPCR analysis in biodistribution assays constitutes a highly sensitive approach to systemically track cells in vivo. Thereby, human ECFCs administered intramuscularly to CLTI mice remained locally within the ischemic tissues, while intravenously injected cells were found in several organs. Our data

<sup>†</sup>Marta Rojas-Torres and Ismael Sánchez-Gomar both authors contributed equally to this work.

\*Correspondence: [maricarmen.duran@gm.uca.es](mailto:maricarmen.duran@gm.uca.es)

<sup>1</sup> Biomedicine, Biotechnology and Public Health Department, Cádiz University, Cádiz, Spain  
Full list of author information is available at the end of the article



© The Author(s) 2022. **Open Access** This article is licensed under a Creative Commons Attribution 4.0 International License, which permits use, sharing, adaptation, distribution and reproduction in any medium or format, as long as you give appropriate credit to the original author(s) and the source, provide a link to the Creative Commons licence, and indicate if changes were made. The images or other third party material in this article are included in the article's Creative Commons licence, unless indicated otherwise in a credit line to the material. If material is not included in the article's Creative Commons licence and your intended use is not permitted by statutory regulation or exceeds the permitted use, you will need to obtain permission directly from the copyright holder. To view a copy of this licence, visit <http://creativecommons.org/licenses/by/4.0/>. The Creative Commons Public Domain Dedication waiver (<http://creativecommons.org/publicdomain/zero/1.0/>) applies to the data made available in this article, unless otherwise stated in a credit line to the data.

corroborate the need to perform biodistribution assays in order to define specific parameters such as the optimal delivery route for ECFCs before their application into the clinic.

**Keywords:** Biodistribution, CLTI, Cell therapy, ECFCs, DiR labeling

## Background

Critical limb-threatening ischemia (CLTI) constitutes a debilitating disease caused by the narrowing and obstruction of the primary systemic arteries, mainly due to atherosclerosis. CLTI patients suffer from chronic rest pain, ischemic ulcers, gangrene and, eventually, toes or extremities amputation, significantly impairing their quality of life [1, 2]. The prevalence and incidence of this disease is constantly growing, representing a great burden for public health [3]. Despite significant advances in surgical treatments (i.e., bypass or angioplasties) [4], the percentage of patients that could undergo surgical revascularization is low, principally due to related comorbidities [5, 6]. In addition, some patients require re-intervention and, in the last term, they might need amputation. Alternatively, angiogenic cell therapy has emerged as a feasible option for ischemic diseases because of its potential to enhance revascularization and blood flow recovery, returning oxygen and nutrients towards the affected areas [7–9]. Different strategies, including the administration of endothelial colony-forming cells (ECFCs), are currently under investigation, mainly with “no-option” CLTI patients [10]. ECFCs have the ability to augment collateral revascularization and reperfusion [11, 12], representing a suitable candidate to treat ischemic diseases such as CLTI.

Before these and other cell treatments can be translated into the clinic, several preclinical assays are required by regulatory authorities to ensure the safety and efficacy of cell-based medicinal products [13, 14]. These therapies should guarantee the highest cell availability for therapeutic effects within the target tissue, as well as the avoidance of possible undesirable effects as result of the translocation to other parts of the body. Therefore, cell tracking assays are required to decipher the systemic biodistribution of cells, which might depend, among others, on the injection route. Likewise, other factors such as cell size or source, immunological features and labeling, detection method or the animal model could also affect the pharmacokinetics of cells [15].

Currently, multiple cell-tracking strategies are applied. Amid all, cell transfection with fluorescent proteins allows visualization via microscopy and provides quantitative information regarding cell localization [13]. However, the transfection efficacy might affect cell expression and further follow-up at the long term [16, 17]. Alternatively, the use of nanoparticles for cell labeling does not

compromise intrinsic cell processes and offer adequate spatial resolution, although these methods require specific equipment and trained personnel, not always applicable to all facilities [18, 19]. Instead, optical imaging is widely used in preclinical models, providing excellent sensitivity without cell compromising or without high-tech equipment requirements. In this regard, fluorescence and bioluminescence are the two major methods applied [20–23]. The near-infrared (NIR) dye carbocyanine 1,1-dioctadecyl-3,3,3,3-tetramethylindotricarbocyanine iodide (DiR) has been commonly used with a variety of cells, including mesenchymal stem cells (MSCs) [24, 25], macrophages [26, 27], cardiospheres [28], extracellular vesicles [29] or epithelial cells [30]. This lipophilic NIR fluorescent dye gets inserted into cell membranes resulting in a specific and stable signal as a result of high cellular uptake. Moreover, NIR properties are beneficial for *in vivo* cell imaging and tracking, due to reduced animal auto-fluorescence at higher wavelength [31, 32]. Its lipophilic condition makes cell labeling requirements equivalent to physiological environment, not damaging cell viability. Despite all this, a thorough optimization of the labeling protocol is required, as any residual dye remaining in the injection solution could stain other tissues and provide false positive fluorescent signals.

Herein, we have performed an optimized DiR labeling protocol for ECFCs, to avoid any false positive signals during preclinical biodistribution assays. Furthermore, this strategy was applied to compare two alternative biodistribution routes for ECFCs, intramuscular (IM) and intravenous (IV) administration, in a murine model of CLTI, evaluating, simultaneously, two complementary strategies for cell tracking: DiR labeling and qPCR amplification of specific Alu sequences, as previously described [33–35].

## Methods

### ECFCs isolation, culture and characterization

ECFCs were isolated from human umbilical cord blood as described [36–38] and cultured in 1% gelatin-coated plates using ECFCs-medium: EGM-2 (except for hydrocortisone; Lonza) supplemented with 20% FBS, 1X Penicillin/Streptomycin (P/S). ECFCs between passages 5 and 7 were used for all experiments.

Cell identity was confirmed by testing cloning-forming ability, as described [39]. Also, several markers were analyzed by flow cytometry with the Cytotflex (Beckman

Coulter) cytometer and CytoExpert software: CD14, CD31, CD34, CD45, CD73, CD90, CD133, CD146 and CD309. An isotype IgG1 antibody was used as a negative control. Data were analyzed with FlowJo v10.4 software. The full list of antibodies can be found in supplementary materials (Additional file 1: table S1), as well as the results of ECFCs characterization by flow cytometry (Additional file 1: figure S1).

### Animals

Balb-C Nude (CAN.N.Cg-Foxn1nu/Crl) mice (n:16), age 9–12 weeks, male and female (in equal numbers), were produced and maintained under standard laboratory conditions at the Animal Core Facility (SEPA), Cadiz University. Mice were allocated in special rooms, with technical staff constantly supervising filters and air recirculation and monitoring any signs of ill-health. Animals were fed sterile standard chow diet ad libitum and had free access to sterile water. No animal was sacrificed prematurely during the experiments.

### Optimization of DiR labeling

#### *Determination of the relation between DiR intensities and cell numbers*

First, a standard curve was designed to determine the number of cells based on DiR intensity values. Thus,  $1 \cdot 10^6$  ECFCs were labeled with  $6.67 \mu\text{M}$  DiR (Biotium, #60,017) in 1 ml of PBS 1X during 25 min at  $37^\circ\text{C}$ , following standard guidelines. After that, three consecutive washing steps were performed with 1 ml of PBS 1X, including centrifugation (5 min, 500 g), discarding supernatants and washing cells. Next, different amounts of ECFCs (1/2 serial dilutions) were seeded in a 12-well plate: 200,000, 100,000, 50,000, 25,000, 12,500, 6250, 3125, 1562 and 781 cells. The plate was scanned in the Odyssey image NIR acquisition system (Licor Biosciences). Parameters used for the scan: Intensity 2 and detectors in 700 nm and 800 nm activated. Intensity values were registered on day 1, day 2 and day 3 after seeding as K counts/ $\text{mm}^2$ , and standard curves were obtained per day (in triplicates) with excel.

#### *Determination of the optimal DiR staining protocol*

We next evaluated whether the solution remaining from the three washing steps after DiR labeling could still stain other cells. In total,  $1 \cdot 10^6$  ECFCs were labeled with  $6.67 \mu\text{M}$  DiR in 1 ml of PBS 1X, 25 min,  $37^\circ\text{C}$ . Cells were centrifuged (5 min, 500 g), the supernatant was collected in a new tube, and cells were washed with 1 ml of PBS 1X. This washing step was repeated twice, collecting also the supernatants from each wash. Then,  $2 \cdot 10^5$  and  $1 \cdot 10^5$  ECFCs from the initial DiR labeling (and after three consecutive washes) were seeded in a 12-well plate.

Additionally, other sets of ECFCs ( $1 \cdot 10^5$ ) were incubated each one with the solutions collected from the three consecutive washing steps, 25 min at  $37^\circ\text{C}$ , plated and scanned as previously indicated to determine residual staining (Fig. 1A).

Next, we proceeded as before, incubating  $1 \cdot 10^6$  cells with DiR  $6.67 \mu\text{M}$  in 1 ml of PBS 1X, 25 min at  $37^\circ\text{C}$ , but washing three times with 10 ml of PBS 1X. Again, supernatants from each washing step were collected and ECFCs ( $1 \cdot 10^5$ ) were incubated with them, to determine if the remaining DiR solution could still preserve the capacity to stain cells (Fig. 1B).

#### *Determination of DiR residual concentrations*

In order to calculate the concentration of DiR equivalent to the one observed in cells pre-labeled with the third wash step (residual DiR), a standard curve was built by incubating ECFCs ( $1 \cdot 10^5$ ), 25 min and  $37^\circ\text{C}$ , with serial DiR dilutions (1/2), ranging from  $3.34 \mu\text{M}$  up to  $0.0016 \mu\text{M}$ . Cells were scanned as described above, together with a negative control, consisting of  $1 \cdot 10^5$  unlabeled cells, to consider background levels.

#### *Determination of DiR residual staining concentrations in vivo and ex vivo*

Afterward, we tested whether the DiR residual intensity detected in vitro could also have any signal in vivo (Fig. 1C). Again,  $1 \cdot 10^6$  ECFCs were labeled with  $6.67 \mu\text{M}$  DiR, 25 min at  $37^\circ\text{C}$ , followed by three washing steps with 10 ml PBS 1X. After centrifugation, the supernatant from the third wash (DiR residual) was collected. Balb-c nude mice (n:5) were anesthetized administering intraperitoneally xylazine (10 mg/kg) and ketamine (100 mg/kg), and  $1 \cdot 10^6$  DiR-labeled ECFCs (resuspended in 50  $\mu\text{l}$  sterile saline serum) were injected intravenously (via tail, IV+) or intramuscularly (left hind limb, IM+) as positive controls. In addition, another set of mice were injected, intravenous (IV-) and intramuscularly (IM-), with  $0.2 \mu\text{M}$  of DiR, equivalent to the third wash (DiR residual). Finally, a negative control with  $1 \cdot 10^6$  unlabeled ECFCs was used to consider background signals (NC).

On day 0 and day 1 after cell administration, mice were anesthetized and transferred to the NiR scanning system (Odyssey, LI-COR Biosciences), and in vivo images were taken, registering the DiR intensities from the areas of thorax, abdomen, both limbs and paws. Mice were sacrificed in a  $\text{CO}_2$  chamber (day 1), and several tissues and organs were extracted: left and right limbs, spleen, kidneys, liver and lungs. They were all immediately scanned with the parameters indicated above.

DiR fluorescence values from in vivo and ex vivo assays were calculated per organ/area of scanned regions. Experimental values were normalized *versus* the NC,

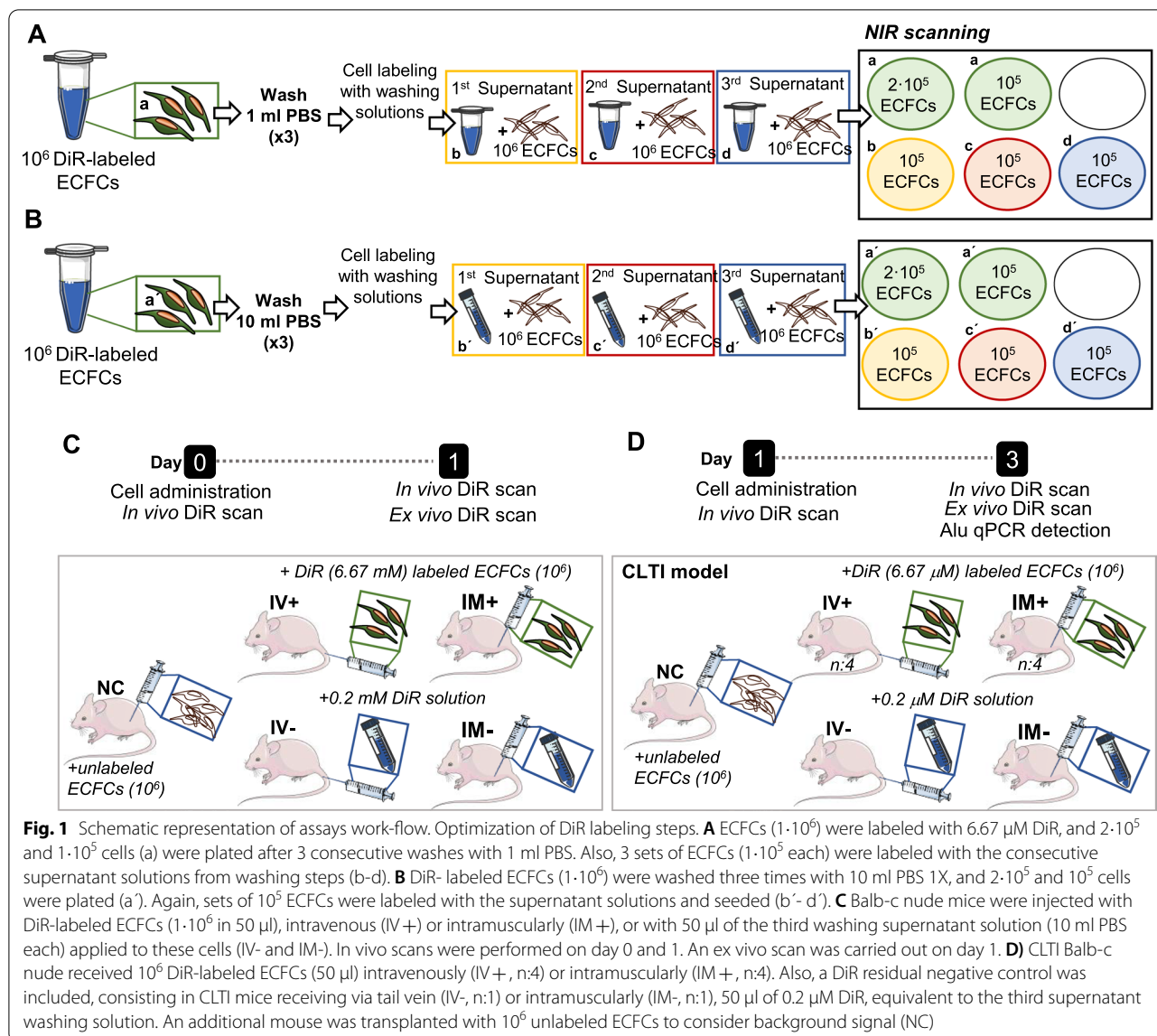


**Fig. 1** Schematic representation of assays work-flow. Optimization of DiR labeling steps. **A** ECFCs ( $1 \cdot 10^6$ ) were labeled with  $6.67 \mu\text{M}$  DiR, and  $2 \cdot 10^5$  and  $1 \cdot 10^5$  cells (a) were plated after 3 consecutive washes with 1 ml PBS. Also, 3 sets of ECFCs ( $1 \cdot 10^5$  each) were labeled with the consecutive supernatant solutions from washing steps (b-d). **B** DiR-labeled ECFCs ( $1 \cdot 10^6$ ) were washed three times with 10 ml PBS 1X, and  $2 \cdot 10^5$  and  $10^5$  cells were plated (a). Again, sets of  $10^5$  ECFCs were labeled with the supernatant solutions and seeded (b-d). **C** Balb-c nude mice were injected with DiR-labeled ECFCs ( $1 \cdot 10^6$  in  $50 \mu\text{l}$ ), intravenous (IV+) or intramuscularly (IM+), or with  $50 \mu\text{l}$  of the third washing supernatant solution (10 ml PBS each) applied to these cells (IV- and IM-). In vivo scans were performed on day 0 and 1. An ex vivo scan was carried out on day 1. **D** CLTI Balb-c nude received  $10^6$  DiR-labeled ECFCs ( $50 \mu\text{l}$ ) intravenously (IV+, n:4) or intramuscularly (IM+, n:4). Also, a DiR residual negative control was included, consisting in CLTI mice receiving via tail vein (IV-, n:1) or intramuscularly (IM-, n:1),  $50 \mu\text{l}$  of  $0.2 \mu\text{M}$  DiR, equivalent to the third supernatant washing solution. An additional mouse was transplanted with  $10^6$  unlabeled ECFCs to consider background signal (NC)

which was taken as baseline (0 intensity) and after that fluorescence intensity values of IV- and IM- (residual DiR negative controls) were subtracted from IV+ and IM+ intensities. Fluorescent intensities were registered as counts/mm<sup>2</sup>. Full information regarding fluorescence intensities in vivo and ex vivo can be found in Additional file 1: Tables S2-S3.

**In vitro analysis and biocompatibility**

**Proliferation assay**

DiR-labeled ( $6.67 \mu\text{M}$  DiR) and unlabeled  $1 \cdot 10^5$  ECFCs (n:4) were plated in 12-well plates pre-coated with 1% gelatin, and cultured in ECFCs-medium for 48 h, as described above. Next, cells were fixed in 4%

paraformaldehyde (PFA), permeabilized with 0.2% triton and blocked with 5% BSA and 0.1% triton, followed by incubation with the primary antibody anti- $\alpha$ -Ki67 (1:500, PA5-16,785, Invitrogen), at 4 °C overnight, and then with the specific secondary antibody (1:500, A-21428, ThermoFisher), 1 h, at room temperature in the dark. Finally, nuclei were stained with DAPI ( $0.2 \mu\text{g/ml}$ ). Images were acquired from random sections (n:5) of each well, using MMI CellCut Plus (Olympus), at 20X magnification, and then analyzed with the Zen 2 (Zeiss) software. The proliferation assay as well as the other in vitro assays was performed with ECFCs from one single donor, repeated four times. The results were expressed as the percentage of total ECFCs that were positive for Ki67.



### **Angiogenesis assay**

Briefly,  $1 \cdot 10^4$  DiR-labeled or untreated ECFCs (n:4) were seeded, in triplicates, into a  $\mu$ -plate angiogenesis 96 well (ibidi, 89,646) pre-coated with 10  $\mu$ l Matrigel (BD Bioscience, 256,231), as described [39]. Images were registered after 24 h, 48 h and 72 h, with a MotiCam 3.0 camera connected to an inverted phase-contrast microscope, under 4X magnification. The number of meshes and total length of segments in each well were quantified using the Angiogenesis Analyzer plugin with Image J v.2.0.

### **Apoptosis assay**

ECFCs ( $1.5 \cdot 10^5$ ) were labeled with 6.67  $\mu$ M DiR (n:4) or left unlabeled (n:4) and then seeded in triplicates in 12-well plates, and cultured 48 h at 37°C, 5% CO<sub>2</sub>. Cells were detached with trypsin and incubated with 5  $\mu$ l propidium iodide (PI, #556,463, BD) and 5  $\mu$ l Annexin-V (AV, PB-V450, #56,056, BD) at 4 °C, 30 min, as described [39]. Apoptotic cells were analyzed by flow cytometry as indicated above.

### **Co-culture assay**

ECFCs ( $1 \cdot 10^5$ ) were labeled with 6.67  $\mu$ M DiR, washed with 10 ml PBS 1x, as described above, seeded in a 1% gelatin-coated 12-well plate and then incubated for 24 h, 37 °C, 5% CO<sub>2</sub> in ECFCs-medium. In parallel, Jurkat cells were grown in RPMI medium supplemented with 10% FBS, 1X P/S, 20% glutamine, collected and washed twice with PBS 1X, and then plated with the pre-labeled ECFCs, co-culturing Jurkat and DiR ECFCs labeled cells in the aforementioned ECFCs conditions. After 24 h, Jurkat cells were collected and labeled with PE-  $\alpha$ -human CD3 antibody (Biolegend, #317,308), 25 min at 4 °C. Also, ECFCs were collected through trypsinization and labeled with  $\alpha$ -human CD31 antibody (Biolegend, #303,103). Fluorescence was measured by flow cytometry, as described above. The mean fluorescence intensities were registered and the percentage of DiR + cells was calculated.

### **Biodistribution assays of ECFCs in CLTI mice**

#### **Murine model of CLTI and administration of DiR pre-labeled ECFCs**

Balb-c nude mice (n:11) were anesthetized with xylazine (10 mg/kg) and ketamine (100 mg/kg), administered intraperitoneally before surgery, and double ligation was performed occluding the distal and proximal ends of the left femoral artery with double knots of suture (non-absorbable 6/0), as previously described [33, 34, 40]. Mice received ketoprofen (2 mg/kg) intraperitoneally as analgesic for three consecutive days.

Twenty-four hours after surgery, eight sets of  $1 \cdot 10^6$  ECFCs were pre-labeled as indicated before

(6.67  $\mu$ M DiR), washing three times with 10 ml PBS. Then, CLTI mice were injected with  $1 \cdot 10^6$  DiR-labeled cells (in 50  $\mu$ l sterile saline serum) either intravenously (via tail, IV +, n:4) or intramuscularly (IM +, n:4), with 3–4 injections in different points (back and front) around the femoral artery. Also, another 2 mice were injected with 0.2  $\mu$ M of residual DiR as negative control (IV-, IM-), together with a NC mouse, with unlabeled cells (Fig. 1D).

### **Near-infrared scanning and data analysis**

In vivo scans were performed on day 1 and day 3 as described before, registering the DiR signal intensities from the areas of thorax, abdomen, as well as both limbs and paws. On day 3, after the in vivo scanning, mice were sacrificed in a CO<sub>2</sub> chamber, and several tissues and organs were extracted and scanned, as indicated above. DiR fluorescence values from in vivo and ex vivo assays were calculated as described in the previous section “Determination of DiR residual staining concentrations in vivo and ex vivo”.

Following the scanning, muscles from the back (gastrocnemius and sole muscle) and front side (tibialis) of the left and right limb surrounding the femoral artery were extracted and snap-frozen in liquid nitrogen for further qPCR analysis of human-specific Alu (hAlu) sequences or fixed in 4% PFA for further immunohistochemistry (IHC).

### **qPCR-Alu sequence analysis**

The presence of human cells (hcells) within the tissues was also determined by quantification of specific hAlu sequences, as previously described [33–35]. Briefly, snap-frozen tissues were homogenized before genomic DNA isolation from tissue samples (hind limbs, kidney, liver, lungs and spleen) using E.Z.N.A Tissue DNA Kit (OMEGA bio-tek).

Linearity and resolution limits were determined by mixing human genomic DNA with murine DNA at several concentrations of human DNA (hDNA) in 100 ng of total genomic DNA. The sensitivity of the assay allowed to detect 1 human cell in 10,000 mouse cells. Alu-qPCR was performed, in triplicates, using TaqMan Universal Master Mix II, no UNG (Thermo Fisher Scientific), 0.2  $\mu$ M forward and reverse primers and 0.25  $\mu$ M hydrolysis probe on a CFX Connect Real-Time System (Bio-Rad), as described [33–35]. Data were analyzed with CFX Manager 3.1 (Bio-rad).

The total number of ECFCs in the different organs was estimated as previously described [33–35]. Values obtained for hDNA in 100 ng were extrapolated to total hDNA extracted per mg of tissue and considering the relation of 5 pg of DNA per hcells, as described [41].

### Detection of DiR-labeled cells by immunohistochemistry

ECFCs distribution among the ischemic tissues was also evaluated by IHC. Thus, frontal tissues from left limbs extracted three days after cell administration were fixed with 4% PFA for 72 h and dehydrated before OCT embedding. Tissues were then transversally sectioned (8  $\mu\text{m}$ ) and IHC was performed to detect endothelial human cells and blood vessels with specific antibodies against CD31 and  $\alpha$ -smooth muscle actin ( $\alpha$ -SMA), respectively, as described [33, 34]. Full information regarding the antibodies employed can be found in Additional file 1: Table S1. Images were taken at 40 $\times$  using a Zeiss LSM 880 confocal microscope. Images were analyzed and processed with the Zen 2 (Zeiss) software.

### Statistical analysis

Statistical analysis was performed using GraphPad Prism v.9 software. Data were verified for normal distribution using Shapiro–Wilk normality test. Differences between groups were calculated with Kruskal–Wallis test and Dunn's test as post hoc analysis. Data were represented as the mean  $\pm$  SEM, indicating the individual points for each data set. Differences were considered as statistically significant with  $p$ -values  $< 0.05$ . Full information including  $p$ -values from each data set analysis is shown in Additional file 1: Tables S4–S12.

## Results

### Optimization of the DiR labeling protocol

#### Relation between DiR intensities and cell numbers

The standard curve designed to determine the number of ECFCs based on DiR intensity values showed a clear correlation between cell number and DiR fluorescent signal (Fig. 2A). This relation remained with time, with  $R^2$  values  $> 0.99$  during three consecutive days (Fig. 2B). Thereby, considering these results, these linear equations were applied later on to determinate cell numbers based on DiR intensity values.

### Determination of the DiR residual staining

The DiR fluorescent signals of ECFCs stained with the residual solution derived from three consecutive washing steps (1 ml PBS 1X/wash) (Fig. 2C) were similar to the strong intensities registered for ECFCs ( $1 \cdot 10^5$ ) directly labeled with standard protocols (direct labeling with 6.67  $\mu\text{M}$  DiR solution and 3 washes with 1 ml PBS). By increasing the washing volume up to 10 ml PBS (Fig. 2D), a significant decrease of DiR signal was seen in ECFCs stained with the residual washing steps, detecting only 10% of the initial DiR seen in pre-labeled cells. In all cases, DiR intensities were proportional to cell numbers, showing half intensity values in the wells with half of cell numbers. Overall, these results indicated that the washes performed with 1 ml PBS 1X each were not sufficient to eliminate the residual DiR, and this could derive into false positive signals during in vivo biodistribution assays. By increasing the washing volume, we removed most of the residual DiR, so we fixed this protocol for future biodistribution assays.

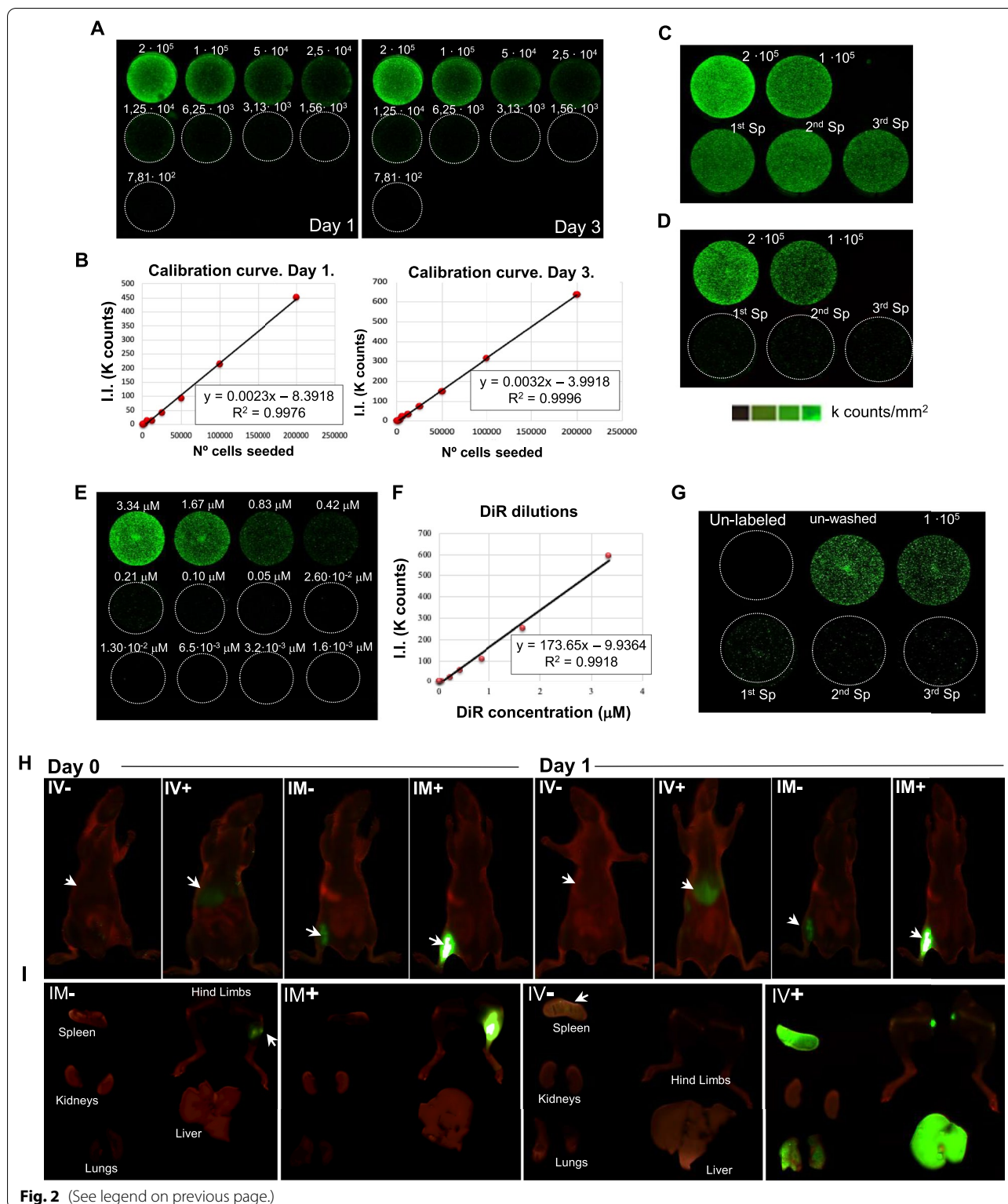
### Determination of the optimal residual concentration for DiR staining

According to the linear equation ( $R^2:0.992$ ) obtained between DiR-cell intensities and DiR concentrations ( $\mu\text{M}$ ) (Fig. 2E–F), the fluorescence detected for ECFCs that did not undergo washing steps (Fig. 2G, second well, top row) correlated to 1.47  $\mu\text{M}$  DiR, while the intensity of the same cells after the third wash (Fig. 2G, third well, top row) correlated to 1.13  $\mu\text{M}$  DiR residual intensities. On the other hand, the DiR intensities of ECFCs incubated directly with the washing supernatants ranged from 0.34  $\mu\text{M}$  (first wash) to 0.19  $\mu\text{M}$  (third wash) (Fig. 2G, lower row), so we fixed 0.2  $\mu\text{M}$  as the DiR residual solution to test in the in vivo assays.

Regarding the in vivo assays, a strong fluorescence signal was seen in mice injected with  $10^6$  ECFCs stained with DiR (6.67  $\mu\text{M}$ ) (intravenously, IV + or intramuscularly, IM +), right after cell administration (Day 0) and on day 1 (Fig. 2H). On the other hand, the mouse

(See figure on next page.)

**Fig. 2** Determination of DiR residual staining. **A** Representative scans from calibration curve on days 1 and 3. ECFCs were incubated with 6.67  $\mu\text{M}$  DiR, plated in  $\frac{1}{2}$  dilutions (from 200,000 cells to 781) and scanned on days 1, 2 and 3. **B** Standard curves (DiR intensity vs cell number) and linear equations obtained for days 1 and 3, corresponding to the averaged values of three independent standard curves performed. **C** Representative images obtained for DiR pre-labeled ECFCs ( $2 \cdot 10^5$  and  $1 \cdot 10^5$ ) (top wells) and ECFCs ( $1 \cdot 10^5$ ) incubated with the 3 consecutive washing solutions (1 ml PBS each) derived from the cells in the upper wells (bottom wells). **D** Scans from Labeled-ECFCs ( $2 \cdot 10^5$  and  $1 \cdot 10^5$ ) (top) and ECFCs ( $1 \cdot 10^5$ ) incubated with the remaining washing solutions (10 ml PBX 1X) from the, (bottom). **E** ECFCs ( $1 \cdot 10^5$ ) were incubated with decreasing amounts of DiR (from 3,34 to  $1.6 \cdot 10^{-3}$   $\mu\text{M}$  DiR, serial dilutions 1/2) **F** Standard curve and linear equation obtained after the incubation of ECFCs with DiR serial dilutions, corresponding to the averaged values of three independent standard curves performed. **G** Scanned plate with ECFCs ( $1 \cdot 10^5$ ), unlabeled (DiR negative control), incubated with 6,67  $\mu\text{M}$  DiR without washing or pre-incubated with 6.67  $\mu\text{M}$  DiR after 3 washes (top row). ECFCs incubated with the supernatant from 3 consecutive washing solutions (lower row). **H** In vivo scans on day 0 (left) and day 1 (right) after administration of 0.2  $\mu\text{M}$  DiR either IV (IV-) or IM (IM-), or administration of  $10^6$  labeled ECFCs (6,67  $\mu\text{M}$  DiR, IV + and IM +). **I** Ex vivo scans of spleen, kidneys, lungs, liver) and hind limbs, one day after injecting either DiR-labeled ECFCs or 0.2  $\mu\text{M}$  DiR. A Negative control (with  $10^6$  unlabeled ECFCs), was also included to discard background signals



injected intramuscularly with 0.2  $\mu\text{M}$  residual DiR (IM-), also reported some signal in the calf muscle on days 0 and day 1. Finally, no fluorescence was detected in vivo

after injecting the residual DiR solution intravenously (IV-), although some signals appeared in the spleen and the liver after the ex vivo scans (Fig. 2I). These results

indicate that DiR can stain tissues even in the absence of cell administration. Therefore, biodistribution assays should include a negative control with DiR residual solution (apart from a negative control with unlabeled cells).

#### DiR staining does not affect ECFCs viability or vessel formation properties

Functional assays confirmed that DiR staining did not affect ECFCs proliferation or viability (Fig. 3A–B). Similarly, ECFCs angiogenic potential was not affected as result of labeling them with DiR, as indicated in a matrigel tubule formation assay in vitro (Fig. 3C). The number of meshes and the total length of the tubules formed was similar in both, labeled and DiR labeled ECFCs, with no significant differences between them (Fig. 3D). Finally, while a strong signal was detected for DiR-labeled ECFCs by flow cytometry, no apparent dye transference from DiR-ECFCs to unlabeled Jurkats was seen after 24 h co-culture (Fig. 3E). In vivo assays confirmed the presence of DiR-labeled ECFCs within the limbs, corroborated by colocalization with human CD31 + staining. Moreover, DiR-labeled ECFCs were also found within the vessels (Fig. 3F).

#### Biodistribution assays after ECFCs administration in a CLTI murine model.

##### Follow up of ECFCs by DiR labeling

Next, we tested the optimized DiR labeling protocol with ECFCs administered either IM or IV to CLTI mice. As a result, one day after IM transplantation, DiR signal was mainly found in the injection area around the ischemic limb ( $p$ -value < 0.05 compared with the other areas except the abdomen). No emission was detected in other areas, such as thorax or abdomen (Figs. 4A–B). By day 3, the DiR-related intensity within the injection area decreased ( $p$ -value < 0.01), although no apparent translocation to other organs was seen (Figs. 4A–B).

Based on the calibration curve previously built, these intensities correlated with a high concentration of cells in the left limb after IM administration at day 1 ( $p$ -value < 0.05 compared to the rest areas except for the abdomen), and even more significantly at day 3 ( $p$ -value < 0.01, Fig. 4C). Finally, the ex vivo scans

confirmed the localization of DiR fluorescence signal mostly in the left limb ( $p$ -value < 0.001 vs other tissues/organs) after IM administration.

On the other hand, the DiR signal from ECFCs administered intravenously (IV+) was mainly found in the abdominal area on day 1, followed by the left limb and thorax (Fig. 4A–C). At day 3, DiR intensity levels remained and even increased mainly in the abdomen ( $p$ -value < 0.01 vs the thoracic cavity, and  $p$ -value < 0.05 compared to the right limb) but decreased in the left limb and disappeared in the thoracic area. Finally, a slight fluorescence signal was found in left and right paws (Fig. 4C). The ex vivo scans of IV transplanted mice revealed that the abdomen fluorescence came from the liver and spleen, and a faint emission was also observed in lungs (Fig. 4E–F).

#### qPCR analysis of ECFCs biodistribution

Complementary to the DiR cell-tracking assay, qPCR data confirmed the presence of ECFCs mainly in the back left muscle, 3 days after IM injection ( $668.60 \pm 122.11$  ECFCs/tissue mg;  $p$ -value < 0.01), but also traces of hDNA in lungs, spleen and liver ( $1.72 \pm 0.99$ ;  $1.08 \pm 0.98$ ;  $0.48 \pm 0.08$ ; respectively) (Fig. 4G). On the other hand, hDNA was detected mainly in the spleen after IV injection ( $4.03 \pm 2.29$  ECFCs per tissue mg;  $p$ -value < 0.05 compared with liver and lungs) and in lower quantity in the back muscles adjacent to the femoral artery ( $1.82 \pm 0.99$  ECFCs/tissue mg) (Fig. 4G).

#### Discussion

We and other researchers have already described the beneficial effects of cell therapy in murine models of CLTI, mainly by promoting blood flow perfusion recovery after enhancement of collateral vessel formation [33, 42, 43]. Similarly, the therapeutic effects of endothelial progenitor cells (EPCs) transplantation in different models of ischemia have already been described [11, 12, 44–46], and the potential use of ECFCs to promote revascularization in CLTI patients seems undeniable [47–49]. These cells enhance revascularization by promoting vessel formation and perfusion recovery, alone or in combination with MSCs [8, 50, 51]. Besides, some preclinical studies

(See figure on next page.)

**Fig. 3** DiR labeling does not affect ECFCs functions. **A** Proliferation assays. Representative images of Ki67 + (red) unlabeled (control) and DiR-labeled ECFCs (DiR-ECFCs) (left). Percentage of Ki67 + cells of unlabeled and DiR-ECFCs (right). **B** Apoptosis assay. Representative dot-plots with Annexin V (AV) and propidium iodide (PI) from flow cytometry (top). Percentage of ECFCs and DiR-ECFCs in early (AV + /PI-, left) and late (AV + /PI+, right) apoptosis. **C** Angiogenesis assay. Representative images of matrigel tubule formation results, obtained with phase-contrast microscope (left) and NIR scanning (right). **D** Number of meshes quantified (left) and total tubule lengths (right) measured at 24 h, 48 h and 72 h, for unlabeled and DiR-labeled ECFCs. **E** Flow cytometry histograms obtained to detect DiR signal (APC+) after co-culturing 24 h DiR pre-labeled ECFCs and unlabeled Jurkats. Percentage of DiR+ (APC+) cells detected for DiR-ECFCs and Jurkats after 24 h co-culture. Data were represented as the mean  $\pm$  SEM indicating all independent values. \* $p$ -values < 0.05. **F** Representative IHC images confirming the presence of DiR labeled cells (red) within the tissue, 3 days after administration, colocalizing with human CD31 + (endothelial marker, green, left image) and also detected nearby blood vessels ( $\alpha$ -SMA staining, green)



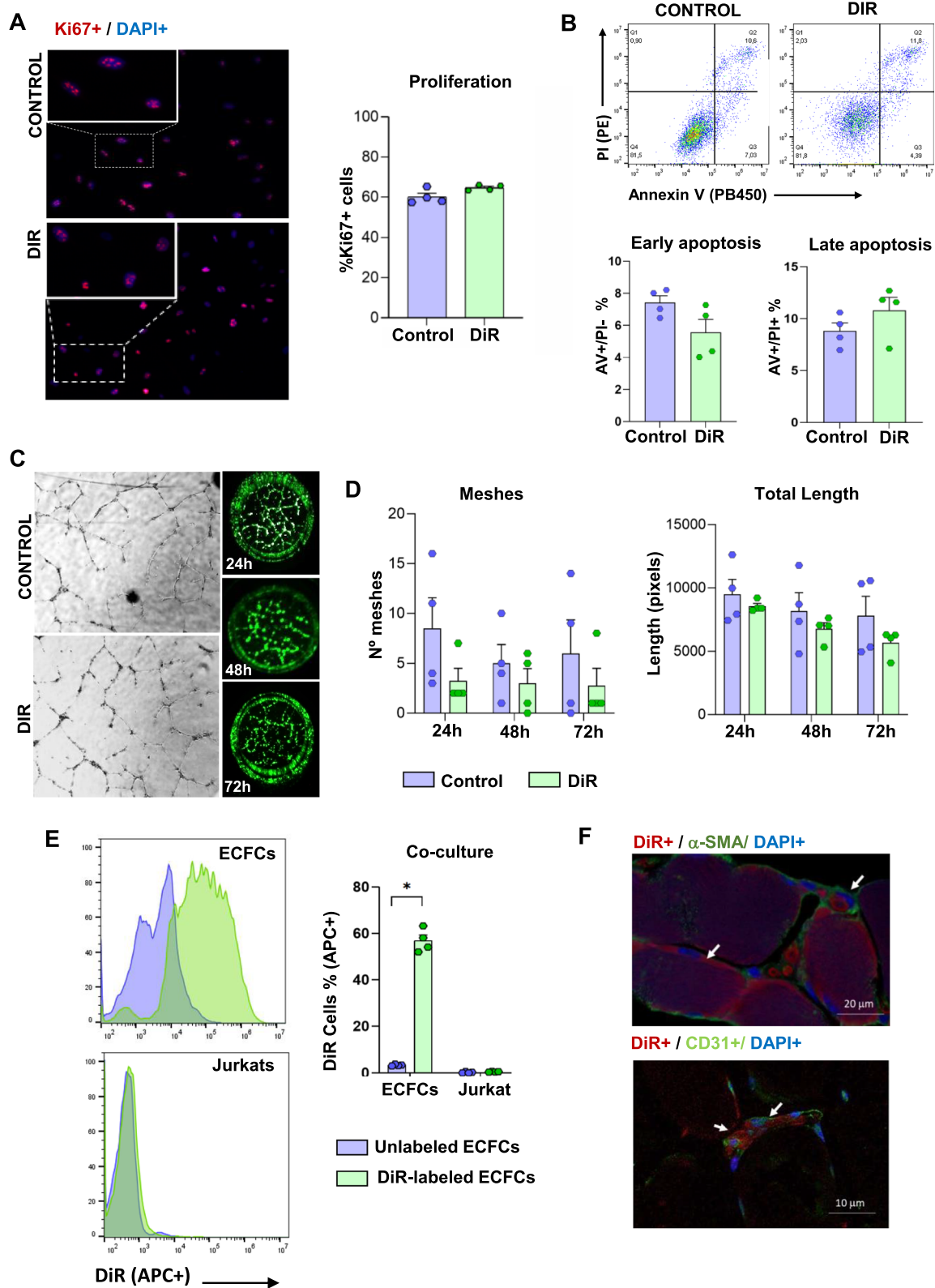


**Fig. 3** (See legend on previous page.)

have already reported a long-term presence of injected ECFCs within the ischemic area, without provoking any adverse effects [12, 51].

Before any potential clinical translation of these cells, several assays are required by regulatory authorities to ensure the safety and efficacy of these potential therapeutic agents [13, 14]. Similarly, other issues as the optimal route of administration and cell biodistribution following transplantation are important concerns to be evaluated. For instance, the delivery route might depend on the cell type or cell dose, and the chosen implantation strategy can significantly affect the therapeutic success [52, 53].

To date, different studies have analyzed the potential of using IM implantation as an alternative to IV in pre-clinical [52, 54] and clinical trials including CLTI patients (i.e., NCT03968198, NCT02993809, NCT04466007; [www.clinicaltrials.gov](http://www.clinicaltrials.gov)). IM implantation has been also compared to intraarterial (IA) cell administration in several clinical studies, presenting similar and/or complementary effects [55–57]. However, most studies targeting CLTI have relied on IM transplantation, most probably because it is less invasive and easier than IA administration [58]. Besides, only a few preclinical assays have been able to reproduce IA administration in animal models [59], mainly due to the difficulty of this approach in small animals.

Herein, we have evaluated, for the first time to our knowledge, which route, either IM or IV administration of ECFCs, could derive in a more focalized delivery of these cells in a CLTI murine model. Our *in vivo* and *ex vivo* DiR and qPCR tracking approach confirmed that after IM administration, ECFCs were retained in the ischemic area, where they were injected, in agreement with other studies using these or other cell types [52, 60–62]. Also, although the DiR assays did not report any apparent translocation to any other organs or tissues, qPCR results reported negligible numbers of hcells in lungs, spleen and liver. We and others have previously described how cells can migrate to the vascular vessels even after IM delivery. Thus, ECFCs might have gone into circulation until the reaching of distal organs, as suggested [63–65].

On the other hand, DiR labeled ECFCs administered intravenously were detected around the abdominal

cavity, less intensively in the left limb and barely in the thorax. The abdominal signal came mainly from the liver and spleen, with some fluorescence also detected in the lungs. These data confirmed the necessity to perform *ex vivo* monitoring together with the *in vivo* cell tracking, in order to avoid signal loss associated with the interference of epithelial layers [59, 66, 67]. Finally, qPCR results corroborated the presence of human ECFCs mainly in the spleen after IV injections, as previously reported [68], and low levels in the liver, where other researchers also found IV-administered endothelial cells [59, 68]. Similarly, cells like bone marrow stromal cells or MSCs are known to accumulate in the lungs when administered IV, with potentially adverse effects [69, 70].

Thus, while health authorities should rule the acceptable number of cells that could be present in nontarget organs, our data corroborated the importance of conducting these approaches to determine the best administration route for a specific cell therapy candidate, prior to any potential translation into the clinic.

Our results also highlighted the importance to complement imaging studies with DNA analysis, to confirm and support imaging-based biodistribution assays [30, 71]. Regarding the two approaches selected here, DiR *in vivo* cell tracking or post-mortem qPCR analysis, they both have their advantages and disadvantages. DiR cell tracking resulted in a successful strategy to provide *in vivo* biodistribution of ECFCs with dependence on the delivery route. Moreover, DiR staining did not affect cell proliferation or viability or their capability to form vessels. Yet, it seems compulsory to consider that although in small extent, probe release or dilution during cell division, cell death or phagocytic events could cause false positive signals. Conversely, qPCR analysis does not provide information “*in vivo*”, but quantification of hDNA using specific Alu sequences has resulted in a highly sensitive approach, with a detection range of 1 human cell in 10,000 mice cells.

Finally, we have shown that, despite many researchers reassuring that DiR does not promote unspecific staining, residual DiR (released during the cell labeling protocol) can significantly stain cells and tissues. This fact can remarkably affect the estimation of cell biodistribution and the determination of cell quantity based solely on

(See figure on next page.)

**Fig. 4** Biodistribution assay after ECFCs administration to CLTI mice. **A** *In vivo* scan on day 1 (top) and day 3 (bottom) after intramuscular (IM +, n:4) or intravenous (IV +, n:4) administration of  $10^6$  DiR pre-labeled ECFCs to CLTI mice. A set of mice injected via tail vein (IV-, n:1) or intramuscular (IM-, n:1) with  $0.2 \mu\text{M}$  DiR solution as residual DiR negative controls were included, together with a Negative Control (with  $1 \cdot 10^6$  unlabeled ECFCs) to consider background signals during the *in vivo* and *ex vivo* scans. **B** Fluorescence intensity (FI) per area ( $\text{k counts}/\text{mm}^2$ ) on days 1 and 3 after IM (top) or IV (bottom) injection of  $1 \cdot 10^6$  DiR pre-labeled ECFCs. **C** Cell number estimation per area ( $\text{cells}/\text{cm}^2$ ) of *in vivo* scans on days 1 and 3 of IM (left) and IV administration (right) ECFCs. **D** *Ex vivo* scans from spleen, kidneys, lungs, liver and hind limbs at day 3 after ECFCs IM or IV transplantation. **E** Fluorescence intensity (FI) per area ( $\text{k counts}/\text{mm}^2$ ) of organs after performing an *ex vivo* scan. **F** Cell number estimation per area ( $\text{cells}/\text{cm}^2$ ) of *ex vivo* scans. **G** Number of cells per tissue mg calculated after human-specific Alu gene amplification by qPCR in liver, spleen, lungs, kidneys and back muscle tissue at day 3

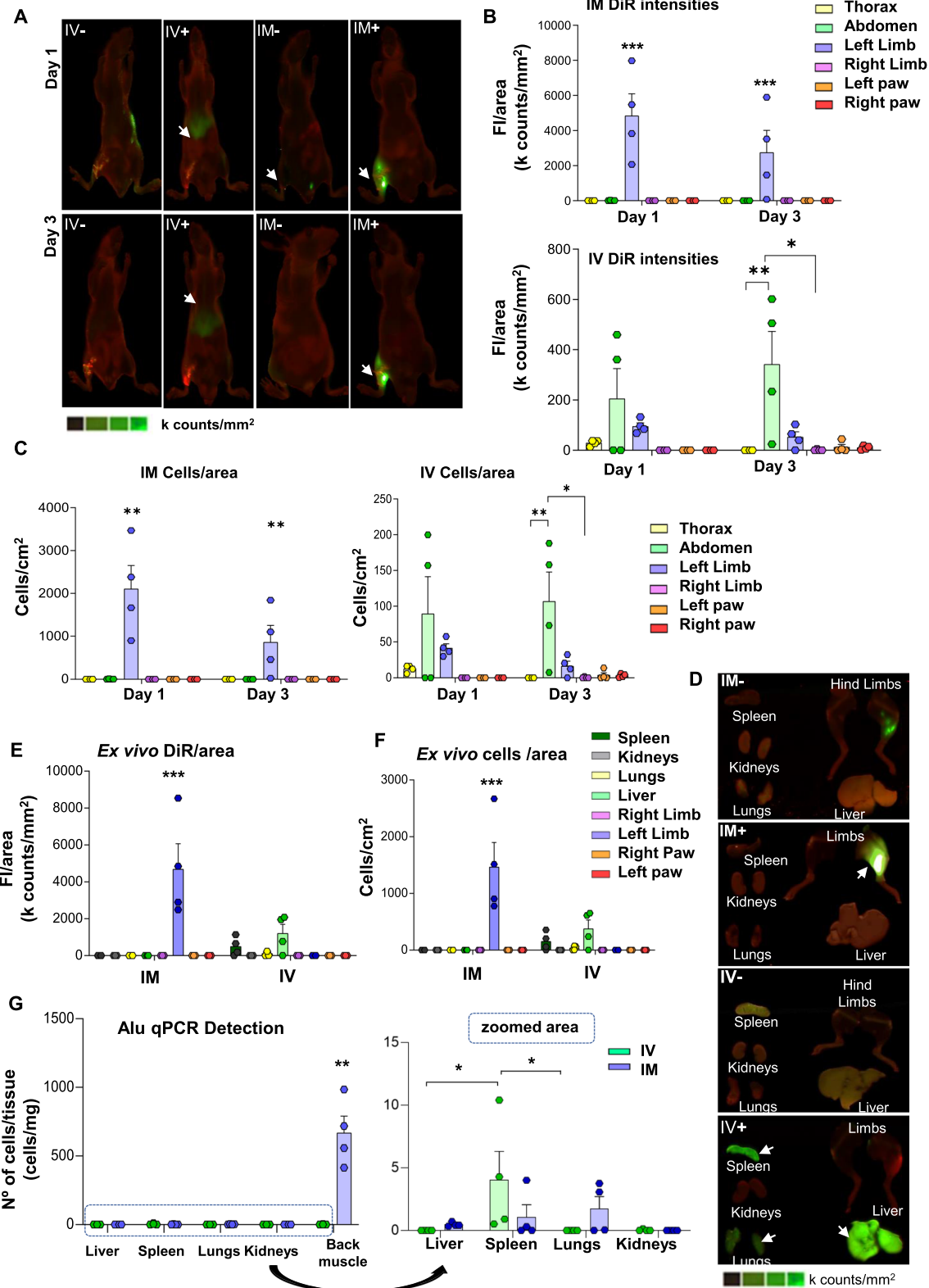


**Fig. 4** (See legend on previous page.)

DiR staining if the effect of un-appropriate labeling protocol (i.e., washing steps) is not considered. Our results indicate that the volume of the washing solution is crucial, with intense signals detected in cells after following the standard procedure applied for DiR labeling. Indeed, the residual dye could still stain cells in similar levels than the original DiR labeling concentration. Thus, astringent washing steps are required to ensure the optimal removal of any residual DiR dye. Likewise, *in vivo* studies including DiR-cell staining have often used mice injected with unlabeled cells as negative controls, without taking into account that DiR alone provides a strong signal by itself. Although we did not detect transference between co-cultured cells *in vitro*, we reported fluorescence in mice injected (IM or IV) with the residual solution (0.2  $\mu$ M DiR), suggesting that a residual DiR negative control should be included in order to discard any false positive signals.

## Conclusion

Herein, we describe an optimized workflow for an accurate *in vivo* and *ex vivo* cell tracking analysis with DiR, a NIR lipophilic labeling dye, for its use in preclinical biodistribution assays. Overall, intensive washing steps and residual DiR negative controls are required in order to properly quantify cells based on DiR labeling, to avoid false positive signals coming from the dye itself, both *in vivo* and *ex vivo*. Also, *in vivo* scans do not provide accurate information regarding the fluorescence intensity signals associated to internal organs, so *ex vivo* scans are necessary to confirm the presence and quantity of cells within the organs of interest. Besides, our results indicate that a combination of *in vivo* DiR imaging with qPCR amplification of human DNA constitutes a highly sensitive approach to track cells systemically.

We have shown that human ECFCs can be efficiently labeled with DiR and tracked *in vivo* and *ex vivo* in immunosuppressed mice. Moreover, according to our results, ECFCs administrated intramuscularly remained mainly within the ischemic limb while those injected intravenously were found in several organs, mostly in the spleen and some traces in the liver. While future studies are warranted to determine the precise durability of the administered DiR labeled cells within the limbs, our data support intramuscular administration of ECFCs in CLTI mice as an optimal strategy to ensure a more focalized distribution and therefore higher availability of the transplanted cells in the ischemic area. Our data support the requirement of biodistribution studies before any potential translation of cell-based therapy approaches into the clinic, in order to obtain an overview of possible

and undesirable cellular translocations outside the areas of interest.

## Abbreviations

AV: Annexin V; CLTI: Critical limb-threatening ischemia; DiR: 1,1-Dioctadecyl 3,3,3,3-tetramethylindotricarbocyanine iodide; ECFCs: Endothelial colony-forming cells; hAlu: Human-specific Alu; hcells: Human cells; hDNA: Human DNA; IM: Intramuscular; IV: Intravenous; MSCs: Mesenchymal stem cells; NIR: Near-infrared; PFA: Paraformaldehyde; PI: Propidium iodide;  $\alpha$ -SMA:  $\alpha$ -Smooth muscle actin.

## Supplementary Information

The online version contains supplementary material available at <https://doi.org/10.1186/s13287-022-02943-8>.

**Additional file 1.** Supplementary Materials. Supplementary Figure S1. Supplementary Tables S1–S12.

## Acknowledgements

We would like to thank the Animal Research Facility from Cadiz University for the assistance provided anytime, and also to Angel García at the SC-ICYT core facility, UCA. Thanks to Prof. Aguado for providing Jurkat cells and his support.

## Author contributions

MR-T and IS-G performed: experimental assays, collection and assembly of data, data analysis and interpretation, manuscript writing and editing. AR-V, LB-C, SE-A and JAA-P: provided support in animal experimental assays and data collection. JM-R participated in: conception, design, data analysis and interpretation. RM-L provided: support in experimental assays, financial support, manuscript review and edition. MD-R participated in: conception and design, provided financial and support, administrative support, participated in collection and assembly of data, data analysis and interpretation and, manuscript writing. All authors read and approved the final manuscript.

## Funding

This study was supported by the Institute of Health Carlos III, ISCIII (PI20-00716, PI18-00427), co-funded by European Regional Development Fund "A way to make Europe"; the "Programa Operativo de Andalucía FEDER, Iniciativa Territorial Integrada ITI 2014–2020 Consejería de Salud (PI0026-2017); and the PAIDI-RETOS (PI20-00932), Junta de Andalucía.

## Data availability

All data generated or analyzed during this study are included in this published article, and its supplementary information files.

## Declarations

### Ethics approval and consent to participate

All animal experimental procedures were approved by the Ethical Committee from the UCA and the Andalusian Committee of animal experimentation (registration number ES110120000210, project number 07-04-2016-043). The current study followed the standard guidelines for animal research included in the Spanish laws (RD 53/2013) as well as the European Regulations (2012/707/UE). Also, ECFCs from cord blood were obtained at the Hospital Complex of Toledo, Spain, with the approval of the local Ethics Committee. Donors provided informed consents and the study followed the principles outlined in the Declaration of Helsinki.

### Consent for publication

Not applicable.

### Competing interests

The authors declare that they have no competing interest.



**Author details**

<sup>1</sup>Biomedicine, Biotechnology and Public Health Department, Cádiz University, Cádiz, Spain. <sup>2</sup>Institute of Research and Innovation in Biomedical Sciences of Cádiz (INIBICA), Cádiz, Spain. <sup>3</sup>Preclinical R&D Department at Ixaka Iberia SL, Seville, Spain. <sup>4</sup>Laboratory of Neuroinflammation, Hospital Nacional de Parapléjicos, SESCAM, Toledo, Spain.

Received: 15 February 2022 Accepted: 7 April 2022

Published online: 21 June 2022

**References**

- Norgren L, Hiatt WR, Dormandy JA, Nehler MR, et al. Inter-society consensus for the management of peripheral arterial disease (TASC II). *J Vasc Surg.* 2007;45(Suppl S):S5-67.
- Conte MS, Pomposelli FB. Society for vascular surgery practice guidelines for atherosclerotic occlusive disease of the lower extremities management of asymptomatic disease and claudication Introduction. *J Vasc Surg.* 2015;61(3 Suppl):1S.
- Nehler MR, Duval S, Diao L, Annex BH, et al. Epidemiology of peripheral arterial disease and critical limb ischemia in an insured national population. *J Vasc Surg.* 2014;60(3):686-95 e2.
- Lichtenberg M, Schreve MA, Ferraresi R, van den Heuvel DAF, et al. Surgical and endovascular venous arterialization for treatment of critical limb ischaemia. *Vasa.* 2018;47(1):17-22.
- Adam DJ, Beard JD, Cleveland T, Bell J, et al. Bypass versus angioplasty in severe ischaemia of the leg (BASIL): multicentre, randomised controlled trial. *Lancet.* 2005;366(9501):1925-34.
- Patel RS. Team approach to critical limb ischemia care and research. *Tech Vasc Interv Radiol.* 2016;19(2):101-3.
- Cobellis G, Silvestroni A, Lillo S, Sica G, et al. Long-term effects of repeated autologous transplantation of bone marrow cells in patients affected by peripheral arterial disease. *Bone Marrow Transplant.* 2008;42(10):667-72.
- Odent Grigorescu G, Preda MB, Radu E, Rosca AM, et al. Combinatorial approach for improving the outcome of angiogenic therapy in ischemic tissues. *Biomaterials.* 2015;60(7):72-81.
- Beltran-Camacho L, Rojas-Torres M, Duran-Ruiz MC. Current status of angiogenic cell therapy and related strategies applied in critical limb ischemia. *Int J Mol Sci.* 2021. <https://doi.org/10.3390/ijms22052335>.
- Duff S, Mafilios MS, Bhounsule P, Hasegawa JT. The burden of critical limb ischemia: a review of recent literature. *Vasc Health Risk Manag.* 2019;15:187-208.
- Dubois C, Liu X, Claus P, Marsboom G, et al. Differential effects of progenitor cell populations on left ventricular remodeling and myocardial neovascularization after myocardial infarction. *J Am Coll Cardiol.* 2010;55(20):2232-43.
- Schwarz TM, Leicht SF, Radic T, Rodriguez-Arabaolaza I, et al. Vascular incorporation of endothelial colony-forming cells is essential for functional recovery of murine ischemic tissue following cell therapy. *Arterioscler Thromb Vasc Biol.* 2012;32(2):e13-21.
- Creane M, Howard L, O'Brien T, Coleman CM. Biodistribution and retention of locally administered human mesenchymal stromal cells: quantitative polymerase chain reaction-based detection of human DNA in murine organs. *Cytotherapy.* 2017;19(3):384-94.
- Reyes B, Coca MI, Codinach M, Lopez-Lucas MD, et al. Assessment of biodistribution using mesenchymal stromal cells: Algorithm for study design and challenges in detection methodologies. *Cytotherapy.* 2017;19(9):1060-9.
- Zhuang WZ, Lin YH, Su LJ, Wu MS, et al. Mesenchymal stem/stromal cell-based therapy: mechanism, systemic safety and biodistribution for precision clinical applications. *J Biomed Sci.* 2021;28(1):28.
- Ansari AM, Ahmed AK, Matsangos AE, Lay F, et al. Cellular GFP toxicity and immunogenicity: potential confounders in vivo cell tracking experiments. *Stem Cell Rev Rep.* 2016;12(5):553-9.
- Tavri S, Vezeridis A, Cui W, Mattery RF. In vivo transfection and detection of gene expression of stem cells preloaded with DNA-carrying microbubbles. *Radiology.* 2015;276(2):518-25.
- Ning X, Bao H, Liu X, Fu H, et al. Long-term in vivo CT tracking of mesenchymal stem cells labeled with Au@BSA@PLL nanotracers. *Nanoscale.* 2019;11(43):20932-41.
- Girard OM, Du J, Agemy L, Sugahara KN, et al. Optimization of iron oxide nanoparticle detection using ultrashort echo time pulse sequences: comparison of T1, T2\*, and synergistic T1-T2\* contrast mechanisms. *Magn Reson Med.* 2011;65(6):1649-60.
- Kim JE, Kalimuthu S, Ahn BC. In vivo cell tracking with bioluminescence imaging. *Nucl Med Mol Imaging.* 2015;49(1):3-10.
- Kircher MF, Gambhir SS, Grimm J. Noninvasive cell-tracking methods. *Nat Rev Clin Oncol.* 2011;8(11):677-88.
- Kim SH, Park JH, Kwon JS, Cho JG, et al. NIR fluorescence for monitoring in vivo scaffold degradation along with stem cell tracking in bone tissue engineering. *Biomaterials.* 2020;258: 120267.
- Ding J, Zhang Y, Wang CX, Li PC, et al. Dual-modality imaging of endothelial progenitor cells transplanted after ischaemic photothrombotic stroke. *Life Sci.* 2019;239: 116774.
- Berninger MT, Mohajerani P, Kimm M, Masius S, et al. Fluorescence molecular tomography of DiR-labeled mesenchymal stem cell implants for osteochondral defect repair in rabbit knees. *Eur Radiol.* 2017;27(3):1105-13.
- Wang M, Liang C, Hu H, Zhou L, et al. Intraperitoneal injection (IP), Intravenous injection (IV) or anal injection (AI)? Best way for mesenchymal stem cells transplantation for colitis. *Sci Rep.* 2016;6:30696.
- Eisenblatter M, Ehrchen J, Varga G, Sunderkotter C, et al. In vivo optical imaging of cellular inflammatory response in granuloma formation using fluorescence-labeled macrophages. *J Nucl Med.* 2009;50(10):1676-82.
- Shan L. Near-infrared fluorescence 1,1-dioctadecyl-3,3,3-tetramethylindotricarbocyanine iodide (DiR)-labeled macrophages for cell imaging. *Molecular Imaging and Contrast Agent Database (MICAD).* Bethesda (MD)2004.
- Zhang J, Wu Z, Fan Z, Qin Z, et al. Pericardial application as a new route for implanting stem-cell cardiospheres to treat myocardial infarction. *J Physiol.* 2018;596(11):2037-54.
- Wiklander OP, Nordin JZ, O'Loughlin A, Gustafsson Y, et al. Extracellular vesicle in vivo biodistribution is determined by cell source, route of administration and targeting. *J Extracell Vesicles.* 2015;4:26316.
- Srinivasan RC, Kannisto K, Strom SC, Gramignoli R. Evaluation of different routes of administration and biodistribution of human amnion epithelial cells in mice. *Cytotherapy.* 2019;21(1):113-24.
- Frangioni JV. In vivo near-infrared fluorescence imaging. *Curr Opin Chem Biol.* 2003;7(5):626-34.
- Lazaro-Ibanez E, Faruqu FN, Saleh AF, Silva AM, et al. Selection of fluorescent, bioluminescent, and radioactive tracers to accurately reflect extracellular vesicle biodistribution in vivo. *ACS Nano.* 2021;15(2):3212-27.
- Rojas-Torres M, Jimenez-Palomares M, Martin-Ramirez J, Beltran-Camacho L, et al. REX-001, a BM-MNC enriched solution, induces revascularization of ischemic tissues in a murine model of chronic limb-threatening ischemia. *Front Cell Dev Biol.* 2020;8: 602837.
- Beltran-Camacho L, Jimenez-Palomares M, Rojas-Torres M, Sanchez-Gomar I, et al. Identification of the initial molecular changes in response to circulating angiogenic cells-mediated therapy in critical limb ischemia. *Stem Cell Res Ther.* 2020;11(1):106.
- Funakoshi K, Bagheri M, Zhou M, Suzuki R, et al. Highly sensitive and specific Alu-based quantification of human cells among rodent cells. *Sci Rep.* 2017;7(1):13202.
- Lin RZ, Chen YC, Moreno-Luna R, Khademhosseini A, et al. Transdermal regulation of vascular network bioengineering using a photopolymerizable methacrylated gelatin hydrogel. *Biomaterials.* 2013;34(28):6785-96.
- Melero-Martin JM, De Obaldia ME, Kang SY, Khan ZA, et al. Engineering robust and functional vascular networks in vivo with human adult and cord blood-derived progenitor cells. *Circ Res.* 2008;103(2):194-202.
- Moreno-Luna R, Munoz-Hernandez R, Lin RZ, Miranda ML, et al. Maternal body-mass index and cord blood circulating endothelial colony-forming cells. *J Pediatr.* 2014;164(3):566-71.
- Eslava-Alcon S, Extremera-Garcia MJ, Sanchez-Gomar I, Beltran-Camacho L, et al. Atherosclerotic pre-conditioning affects the paracrine role of circulating angiogenic cells ex-vivo. *Int J Mol Sci.* 2020. <https://doi.org/10.3390/ijms21155256>.
- Niiyama H, Huang NF, Rollins MD, Cooke JP. Murine model of hindlimb ischemia. *J Vis Exp.* 2009. <https://doi.org/10.3791/1035>.
- Dolezel J, Bartos J, Voglmayr H, Greilhuber J. Nuclear DNA content and genome size of trout and human. *Cytometry A.* 2003;51(2):127-8.

42. Nammian P, Asadi-Yousefabad SL, Daneshi S, Sheikhha MH, et al. Comparative analysis of mouse bone marrow and adipose tissue mesenchymal stem cells for critical limb ischemia cell therapy. *Stem Cell Res Ther*. 2021;12(1):58.
43. Beltran-Camacho L, Jimenez-Palomares M, Sanchez-Gomar I, Rosal-Vela A, et al. Long term response to circulating angiogenic cells, unstimulated or atherosclerotic pre-conditioned, critical limb ischemic mice. *Biomedicines*. 2021. <https://doi.org/10.3390/biomedicines9091147>.
44. Ding J, Zhao Z, Wang C, Wang CX, et al. Bioluminescence imaging of transplanted human endothelial colony-forming cells in an ischemic mouse model. *Brain Res*. 2016;1642:209–18.
45. Goto K, Takemura G, Takahashi T, Okada H, et al. Intravenous administration of endothelial colony-forming cells overexpressing integrin beta1 augments angiogenesis in ischemic legs. *Stem Cells Transl Med*. 2016;5(2):218–26.
46. Dauwe D, Pelacho B, Wibowo A, Walravens AS, et al. Neovascularization potential of blood outgrowth endothelial cells from patients with stable ischemic heart failure is preserved. *J Am Heart Assoc*. 2016;5(4): e002288.
47. Sun Y, Chen S, Zhang X, Pei M. Significance of cellular cross-talk in stromal vascular fraction of adipose tissue in neovascularization. *Arterioscler Thromb Vasc Biol*. 2019;39(6):1034–44.
48. Ramakrishnan VM, Boyd NL. The adipose stromal vascular fraction as a complex cellular source for tissue engineering applications. *Tissue Eng Part B Rev*. 2018;24(4):289–99.
49. Lin RZ, Moreno-Luna R, Munoz-Hernandez R, Li D, et al. Human white adipose tissue vasculature contains endothelial colony-forming cells with robust in vivo vasculogenic potential. *Angiogenesis*. 2013;16(4):735–44.
50. Rossi E, Smadja D, Goyard C, Cras A, et al. Co-injection of mesenchymal stem cells with endothelial progenitor cells accelerates muscle recovery in hind limb ischemia through an endoglin-dependent mechanism. *Thromb Haemost*. 2017;117(10):1908–18.
51. Kang KT, Lin RZ, Kuppermann D, Melero-Martin JM, et al. Endothelial colony forming cells and mesenchymal progenitor cells form blood vessels and increase blood flow in ischemic muscle. *Sci Rep*. 2017;7(1):770.
52. Braid LR, Wood CA, Wiese DM, Ford BN. Intramuscular administration potentiates extended dwell time of mesenchymal stromal cells compared to other routes. *Cytotherapy*. 2018;20(2):232–44.
53. Fath-Bayati L, Vasei M, Sharif-Paghaleh E. Optical fluorescence imaging with shortwave infrared light emitter nanomaterials for in vivo cell tracking in regenerative medicine. *J Cell Mol Med*. 2019;23(12):7905–18.
54. Lee TK, Hwang H, Na KS, Kwon J, et al. Effect of angiogenesis induced by consecutive intramuscular injections of vascular endothelial growth factor in a hindlimb ischemic mouse model. *Nucl Med Mol Imaging*. 2014;48(3):225–9.
55. Van Tongeren RB, Hamming JF, Fibbe WE, Van Weel V, et al. Intramuscular or combined intramuscular/intra-arterial administration of bone marrow mononuclear cells: a clinical trial in patients with advanced limb ischemia. *J Cardiovasc Surg (Torino)*. 2008;49(1):51–8.
56. Davies MG. Critical limb ischemia: cell and molecular therapies for limb salvage. *Methodist Debakey Cardiovasc J*. 2012;8(4):20–7.
57. Soria-Juan B, Escacena N, Capilla-Gonzalez V, Aguilera Y, et al. Cost-effective, safe, and personalized cell therapy for critical limb ischemia in type 2 diabetes mellitus. *Front Immunol*. 2019;10:1151.
58. Gupta NK, Armstrong EJ, Parikh SA. The current state of stem cell therapy for peripheral artery disease. *Curr Cardiol Rep*. 2014;16(2):447.
59. Mao D, Liu J, Ji S, Wang T, et al. Amplification of near-infrared fluorescence in semiconducting polymer nanoprobe for grasping the behaviors of systemically administered endothelial cells in ischemia treatment. *Biomaterials*. 2017;143:109–19.
60. Scarfe L, Taylor A, Sharkey J, Harwood R, et al. Non-invasive imaging reveals conditions that impact distribution and persistence of cells after in vivo administration. *Stem Cell Res Ther*. 2018;9(1):332.
61. Porat Y, Assa-Kunik E, Belkin M, Krakovsky M, et al. A novel potential therapy for vascular diseases: blood-derived stem/progenitor cells specifically activated by dendritic cells. *Diabetes Metab Res Rev*. 2014;30(7):623–34.
62. Agudelo CA, Tachibana Y, Noboru T, Iida H, et al. Long-term in vivo magnetic resonance imaging tracking of endothelial progenitor cells transplanted in rat ischemic limbs and their angiogenic potential. *Tissue Eng Part A*. 2011;17(15–16):2079–89.
63. Hamidian Jahromi S, Davies JE. Concise review: skeletal muscle as a delivery route for mesenchymal stromal cells. *Stem Cells Transl Med*. 2019;8(5):456–65.
64. Vilalta M, Degano IR, Bago J, Gould D, et al. Biodistribution, long-term survival, and safety of human adipose tissue-derived mesenchymal stem cells transplanted in nude mice by high sensitivity non-invasive bioluminescence imaging. *Stem Cells Dev*. 2008;17(5):993–1003.
65. Shahani P, Kaushal A, Waghmare G, Datta I. Biodistribution of intramuscularly-transplanted human dental pulp stem cells in immunocompetent healthy rats through NIR imaging. *Cells Tissues Organs*. 2020;209(4–6):215–26.
66. Kalchenko V, Shvitiel S, Malina V, Lapid K, et al. Use of lipophilic near-infrared dye in whole-body optical imaging of hematopoietic cell homing. *J Biomed Opt*. 2006;11: 050507.
67. Peng X, Li C, Bai Y, Wang X, et al. Noninvasive evaluation of the migration effect of transplanted endothelial progenitor cells in ischemic muscle using a multimodal imaging agent. *Int J Nanomed*. 2018;13:1819–29.
68. Aicher A, Brenner W, Zuhayra M, Badorff C, et al. Assessment of the tissue distribution of transplanted human endothelial progenitor cells by radioactive labeling. *Circulation*. 2003;107(16):2134–9.
69. Makela T, Takalo R, Arvola O, Haapanen H, et al. Safety and biodistribution study of bone marrow-derived mesenchymal stromal cells and mononuclear cells and the impact of the administration route in an intact porcine model. *Cytotherapy*. 2015;17(4):392–402.
70. Leibacher J, Henschler R. Biodistribution, migration and homing of systemically applied mesenchymal stem/stromal cells. *Stem Cell Res Ther*. 2016;7:7.
71. Gianella A, Guerrini U, Tilenni M, Sironi L, et al. Magnetic resonance imaging of human endothelial progenitors reveals opposite effects on vascular and muscle regeneration into ischaemic tissues. *Cardiovasc Res*. 2010;85(3):503–13.

## Publisher's Note

Springer Nature remains neutral with regard to jurisdictional claims in published maps and institutional affiliations.

**Ready to submit your research? Choose BMC and benefit from:**

- fast, convenient online submission
- thorough peer review by experienced researchers in your field
- rapid publication on acceptance
- support for research data, including large and complex data types
- gold Open Access which fosters wider collaboration and increased citations
- maximum visibility for your research: over 100M website views per year

**At BMC, research is always in progress.**

Learn more [biomedcentral.com/submissions](https://biomedcentral.com/submissions)

